Theoretical and Experimental Characteristics of Single V-Groove Guide for *X*-Band and 100 GHz Operation

YAT MAN CHOI, MEMBER, IEEE, DOUGLAS J. HARRIS, AND KIM-FUNG TSANG

Abstract—**A conformal mapping technique for single-groove guide has been discussed and applied to grooves of V-shaped cross section. Experimental measurements at *X*-band and 100 GHz confirm the theoretical predictions. The characteristic equation and scale factor of the fundamental mode have been developed, and its propagation characteristics are given graphically for several normalized groove dimensions.**

I. Introduction

GROOVE GUIDE is potentially attractive as a low-loss waveguide for frequencies above 100 GHz, where the loss characteristics, dimensional tolerances, and power-handling capacity of the more conventional guides such as rectangular waveguide and microstrip become progressively prohibitive. At frequencies above 100 GHz, this guide becomes increasingly attractive, and a complete system in groove guide including generation, transmission, manipulation, and detection could be ideal. This guide as shown in Fig. 1 has previously been analyzed and summarized by a conformal mapping technique [1] which has been applied to guides with grooves of V-shaped cross section [2], and by a transverse resonance technique which has been extended to obtain an approximate but adequate solution for guides with grooves of rectangular cross section [1], [3].

Harris [4] had shown experimentally that the V-groove guide has propagation characteristics very similar to those of the rectangular-groove guide, except that the attenuation was lower and the rejection of higher modes was more effective. However, theoretical analysis is more complex and tedious.

It is well known that waveguide of any shape in cross section can be mapped into a desired shape of cross section for analysis. The transverse resonance technique requires a known form of field expressions in the central groove and evanescent regions. The conformal mapping technique provides a direct analysis on the V-groove guide. The present analytical approach is to transform the V-groove guide into the parallel-wall guide filled with a nonisotropic and nonuniform medium.

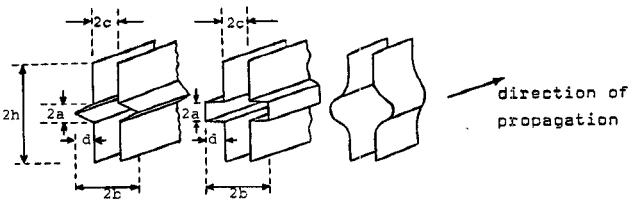

Fig. 1. The grooved waveguide.

II. Conformal Mapping Technique for Single-Groove Guide

A. The Wave Equation for Grooves of Arbitrary Cross Section

The grooved waveguide has been analyzed by a conformal mapping technique [5] which is based on a comparison of a deformed-wall guide containing no dielectric and a real parallel-wall guide filled with a nonisotropic and nonuniform medium (Fig. 2).

The wave equation for the latter guide is given by

$$\nabla_t^2\Phi(x, y) + k_c^2 h^2(x, y)\Phi(x, y) = 0 \qquad (1)$$

where $k_c = \sqrt{k_0^2 - \beta^2}$ is the cutoff wavenumber, $h(x, y)$ is the scaling factor of the conformal transformations between the two coordinate systems, and $\Phi(x, y)$ is the wave function. $\Phi(x, y) = H_z(x, y)$ and $E_z(x, y)$ for TE and TM modes, respectively.

To transform the above solution from the Z space into the U space, we have

$$\begin{bmatrix} h(x, y)\Phi_v \\ h(x, y)\Phi_w \\ \Phi_z \end{bmatrix} = \begin{bmatrix} \Phi_x \\ \Phi_y \\ \Phi_z \end{bmatrix} \qquad (2)$$

Whenever suitable solutions of $\Phi(x, y)$ are found for the pertinent boundary conditions, the transverse components can readily be found by using Maxwell's equations. The

Manuscript received June 5, 1987; revised September 26, 1987. This work was supported in part by the University of Wales Institute of Science and Technology, United Kingdom, and by the Hong Kong Polytechnic, Hong Kong.

Y. M. Choi is with the Department of Electronic Engineering, Hong Kong Polytechnic, Hunghom, Kowloon, Hong Kong.

D. J. Harris was with the University of Wales Institute of Science and Technology, Cardiff, Wales, United Kingdom. He is now with the Department of Electrical and Communication Engineering, University of Technology, Lae, Papua New Guinea.

K.-F. Tsang was with Hong Kong Polytechnic, Hunghom, Kowloon, Hong Kong. He is now with Hewlett Packard Hong Kong Ltd., Hong Kong.

IEEE Log Number 8719435.

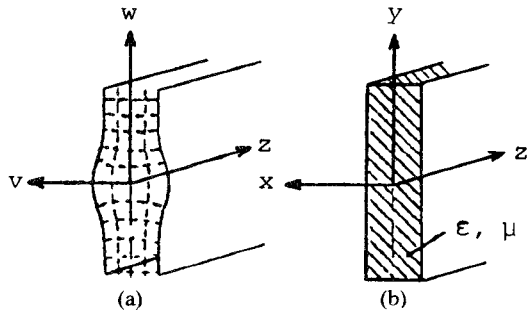

Fig. 2. Parallel-wall waveguide. (a) Deformed-wall guide. (b) Parallel-wall guide with nonuniform and anisotropic medium.

last step in this procedure is to transform the above solution from the Z space into the U space by using (2).

B. Grooves of V-Shaped Cross Section [2]

1) Scaling Factor $h(x, y)$: The scale factor is obtained by using the Schwartz–Christoffel theorem:

$$h(x,y)=\left|\frac{k\pi}{c}\right|\left|\left[\frac{\sin\left[\frac{\pi}{c}(x+jy)\right]-r_0}{\sin\left[\frac{\pi}{c}(x+jy)\right]-1}\right]^{1/2-\theta/\pi}\right| \tag{3}$$

where

$$k=\frac{b}{\int_{-1}^{+1}G(T)\,dT}=\frac{c+ja}{\int_{-1}^{r_0}G(T)\,dT}$$

$$G(T)=\frac{(T-r_0)^{1/2-\theta/\pi}}{(T-1)^{1-\theta/\pi}(T+1)^{1/2}}$$

$$T=\sin\left[\frac{\pi}{c}(x+jy)\right]$$

$$\theta=\tan^{-1}\left(\frac{a}{d}\right).$$

Here a, b, c, and d are the dimensions of the guide as defined in Fig. 1, and x and y represent the coordinates in the parallel-wall guide. The manipulation for obtaining this scale factor is described in the Appendix.

The determination of the constant r_0, which depends on the width $2a$ and depth d of the groove, is tedious, and can be obtained with the following expression:

$$\frac{\int_{-1}^{r_0}G(T)\,dT}{\int_{-1}^{+1}G(T)\,dT}=\frac{c+ja}{b} \tag{4}$$

which is obtained by matching the boundary values before and after the transformation in the complex planes. Plots of r_0 versus $d/2c$, with $2a/2c=0.4$, and of r_0 versus $2a/2c$, with $d/2c=0.6$, are shown in Figs. 3 and 4, respectively. Knowing $h(x, y)$, we can find the longitudinal terms of the relative permeability and permittivity, which permit determination of the field distribution in the groove guide from those in the dielectric-filled parallel-wall guide according to Fig. 2.

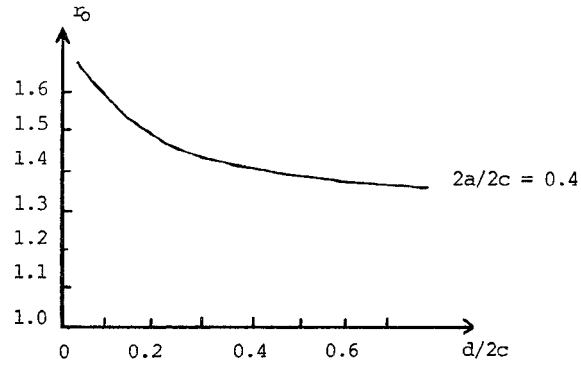

Fig. 3. Graph of r_0 versus normalized groove depth $d/2c$.

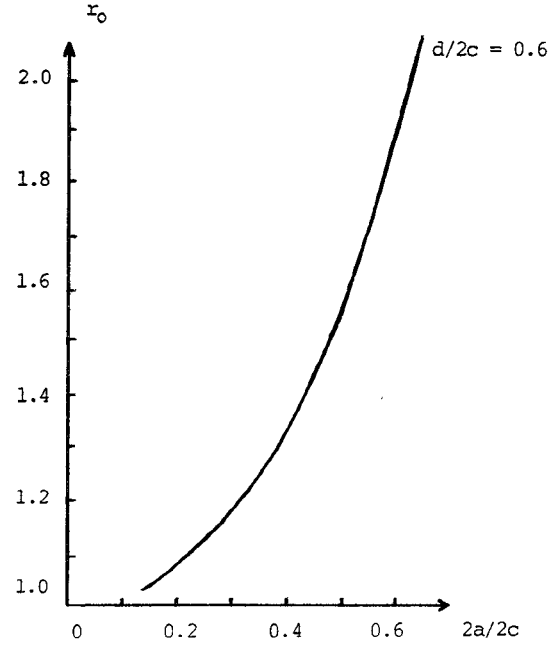

Fig. 4. Graph of r_0 versus normalized groove width $2a/2c$.

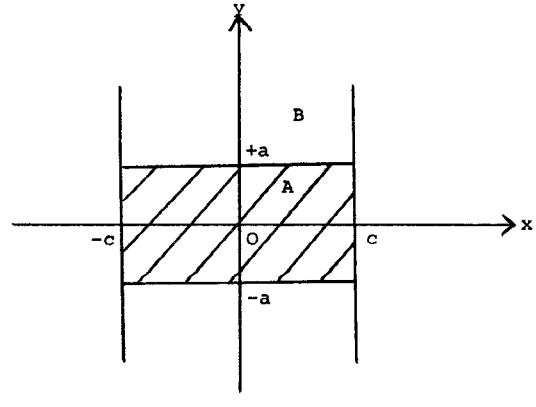

Fig. 5. Cross section of the hypothetical guide.

2) Secular Equation of the TE_0^s Mode: Assume that in region A, where $-a \leqslant y \leqslant a$, the guide is filled with a hypothetical medium as described by (2). In region B, where $y \geqslant |a|$ and $h(x, y)=1$, the guide is uniformly filled (Fig. 5).

The assumed solutions of the wave equation for the TE_0^s modes are expressed below. The factor $\exp(j(\omega t - \beta z))$, which is common to all of the field equations, will be omitted for brevity.

In region A,

$$H_{zA} = \sum_p A_p \sin(k_{xA}x)\cos(k_{yA}y) \tag{5a}$$

and in region B,

$$H_{zB} = \sum_r B_r \sin(k_{xB}x)\exp(-k_{yB}y) \tag{5b}$$

where

- A_p, B_r amplitude constants of field components in regions A and B, respectively,
- k_c $= 2\pi/\lambda_c$, cutoff wavelength of the groove guide,
- λ_c cutoff wavelength,
- k_{xA} $= p\pi/2c$, wavenumber in region A,
- k_{xB} $= r\pi/2c$, wavenumber in region B,
- k_{yA} $< q\pi/2a$, wavenumber in y direction in region A,
- jk_{yB} wavenumber in y direction in region B.

The dimensions of the guide, $2a$ and $2c$, were given in Fig. 1.

Using the first-order approximation ($p = r = 1$), there are the following relations between the wavenumbers:

$$k_{xA}^2 + k_{yA}^2 = K_v k_c^2 \tag{6a}$$

$$k_{xB}^2 - k_{yB}^2 = k_c^2 \tag{6b}$$

where

$$K_v = \frac{1}{2ac\left(\frac{1}{2}+\frac{1}{\pi}\right)} \cdot \int_{-c}^{+c}\int_{-a}^{+a} h^2(x,y)\cos^2\left(\frac{\pi x}{4a}\right)\cos^2\left(\frac{\pi y}{2c}\right)dy\,dx.$$

The boundary conditions imposed between regions A and B ($y = a$) are

(i) $H_{zA} = H_{zB}$ for $-c < x < c$

(ii) $\partial H_{zA}/\partial y = \partial H_{zB}/\partial y$ for $-c < x < c$

(iii) $\partial H_{zA}/\partial y = \partial H_{zB}/\partial y = 0$ at $x = \pm c$.

After applying the boundary conditions to the assumed solution of the wave equation, we obtain the following secular equation:

$$k_{yB} = k_{yA}\tan(k_{yA}a). \tag{7}$$

Equations (6a), (6b), and (7) can be solved for k_{yA}, k_{yB}, and k_c in the first-order approximation.

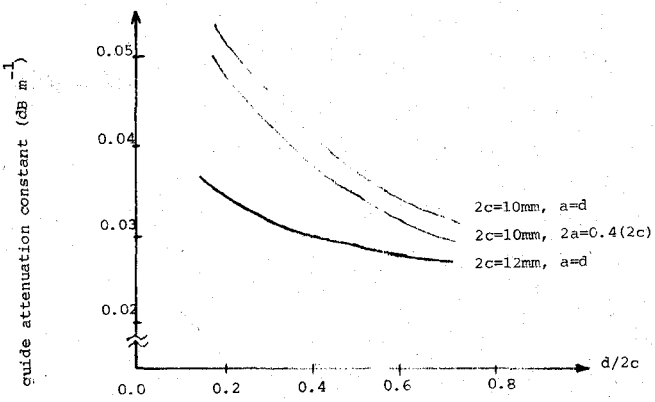

Fig. 6. Graph of guide attenuation constant versus normalized groove depth $d/2c$ at 96 GHz.

III. Propagation Characteristics

A. Attenuation Constant

The attenuation constant for the V-groove guide is given by [5]:

$$\alpha_g = \alpha_{gp}\left[f_c/f_{cp}\right]^4\left[\frac{1-(f_{cp}/f)^2}{1-(f_c/f)^2}\right]^{1/2} G$$

where

- α_{gp} $= \frac{R_s}{Z_0 c}[f_{cp}/f]^2[1-(f_{cp}/f)^2]^{-1/2}$, the attenuation constant of an air-filled parallel-plane waveguide,
- f_{cp} cutoff frequency of the parallel-plane waveguide,
- f_c cutoff frequency of the groove guide,
- f operating frequency,
- G $= A + B(f/f_c)^2[1-(f_c/f)^2]$, a length factor which could be calculated from the wave function and in general $A \gg B$,
- R_s surface resistivity of the guide wall,
- Z_0 intrinsic impedance of free space,
- $2c$ plane separation of the parallel-plane guide,
- A, B constants calculated from the wave function.

A plot of the guide attenuation constant versus $d/2c$ at 96 GHz is shown in Fig. 6. It can be seen that the calculated attenuation constant is very low compared to that of the dominant-mode rectangular waveguide (2 dB/m at 100 GHz).

B. Cutoff Wavelength

Recall from (6b) that the cutoff wavelength λ_c is given by

$$\lambda_c = \frac{2\pi}{\sqrt{\left(\left[\frac{\pi}{2c}\right]^2 + k_{yA}^2\right)/K_v}} = \frac{2\pi}{\sqrt{\left[\frac{\pi}{2c}\right]^2 - k_{yB}^2}}.$$

Fig. 7 shows the cutoff wavelength versus the normalized groove depth $d/2c$. It is seen that the guide is operating well above the cutoff.

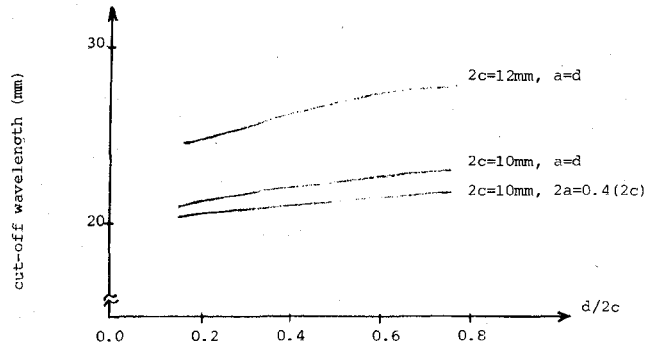

Fig. 7. Graph of cutoff wavelength versus the normalized groove depth d/c.

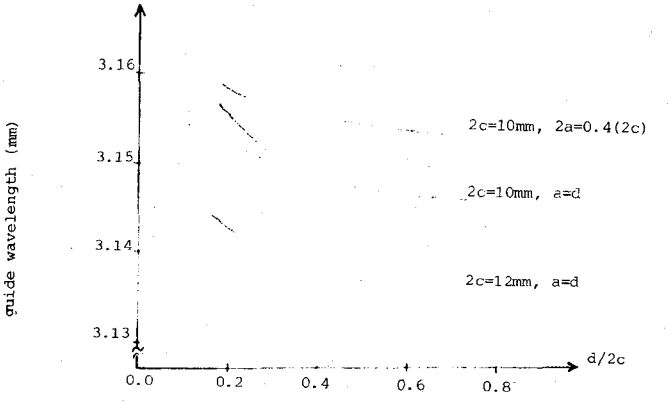

Fig. 8. Graph of guide wavelength versus the normalized groove depth $d/2c$.

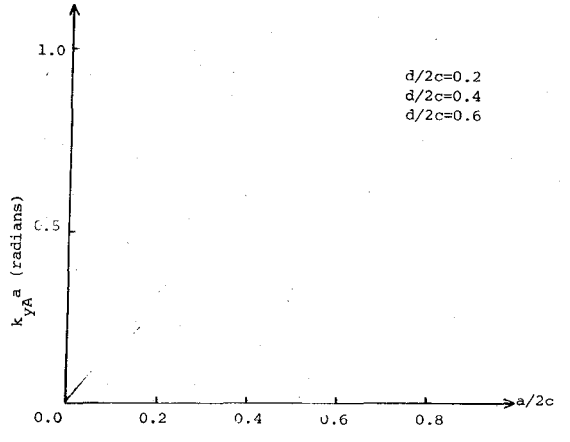

Fig. 9. Product of $k_{yA}a$ versus normalized groove half-width $a/2c$.

C. Guide Wavelength

The guide wavelength λ_g is determined by

$$\frac{1}{\lambda_g^2} = \frac{1}{\lambda_0^2} - \frac{1}{\lambda_c^2}$$

i.e.,

$$\lambda_g = \frac{1}{\sqrt{(1/\lambda_0)^2 - (1/\lambda_c)^2}}.$$

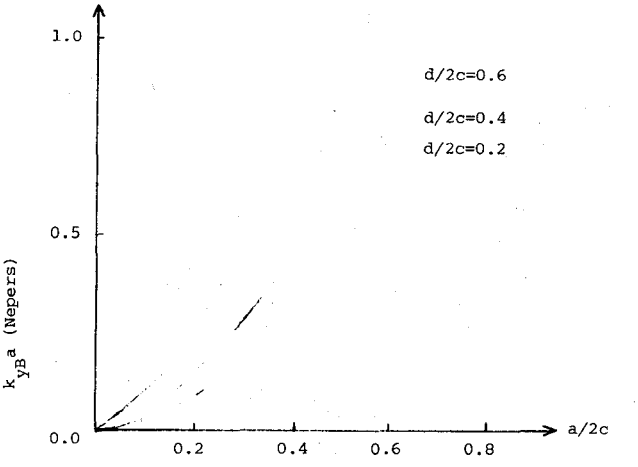

Fig. 10. Product of $k_{yB}a$ versus normalized groove half-width $a/2c$.

Fig. 8 shows the guide wavelength versus the normalized groove depth $d/2c$. It is seen that the theoretical guide wavelength is slightly larger than the free-space wavelength; i.e., the dispersion is low.

D. Wavenumbers

The wavenumbers k_{yA} and k_{yB} can be solved from (6a) and (7). Figs. 9 and 10 show the product of $k_{yA}a$ and $k_{yB}a$, respectively, versus the normalized groove half-width $a/2c$. From Fig. 9 the fraction of a sinusoid across the groove half-width can be determined, while from Fig. 10 the attenuation in the y direction for a distance of half the groove width can be determined.

IV. Measurements of the Propagation Characteristics of Single V-Groove Guide at 100 GHz and at X-Band

Measurement of the guide characteristics at 100 GHz had been made at the University of Wales Institute of Science and Technology, United Kingdom, using a resonance technique with a movable short-circuited plunger [3]. Measurements at X-band were conducted at the Hong Kong Polytechnic, Hong Kong, using a resonance technique with a swept frequency source [2]. A block diagram of the measuring system for single V-groove guide at X-band is shown in Fig. 11 and that at 100 GHz is given in [3].

The experimental and theoretical guide wavelengths λ_g of the guides under test are given in Tables I and II. The correlation between theoretical and experimental values of λ_g is very good indeed (within 0.4 percent at 100 GHz and 3.7 percent at X-band). A graph of guide wavelength versus frequency at X-band is shown in Fig. 12. Since at 100 GHz a movable short-circuited plunger was used, the errors due to the coupling holes of the end plates were removed. Therefore, the error between predicted and measured guide wavelength is significantly higher in X-band than at 100 GHz.

When the measured guide wavelengths λ_g are compared with the operating wavelength λ_o at 100 GHz and at

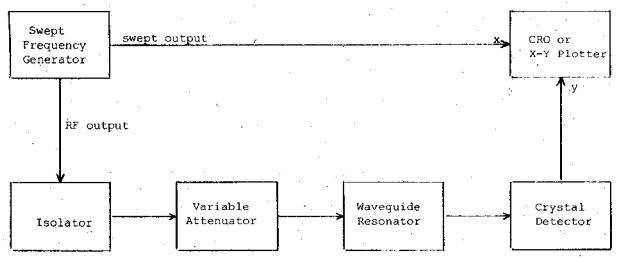

Fig. 11. Block diagram of measuring system for single V-groove guide at *X*-band.

TABLE I
GUIDE WAVELENGTHS AT $\lambda_0 = 3.117$ mm

Guide dimensions(*)		theoretical calculations		experimental results	% of error
2c (mm)	d (mm)	λ_c (mm)	λ_g (mm)	λ_g (mm)	
10	2	20.14	3.155	3.156	0.03
10	4	22.10	3.148	3.146	0.06
10	6	22.51	3.147	3.136	0.35
12	2	24.01	3.144	3.146	0.06
12	4	26.05	3.139	3.138	0.03
12	6	26.84	3.138	3.130	0.26

(*) Other guide dimensions: $2a = 2d$; $2h = 60$ mm.

TABLE II
GUIDE WAVELENGTHS AT *X*-BAND

Guide dimensions (cm)	Theoretical calculations			Experimental results			% of error
	f_o (GHz)	λ_c (cm)	λ_g (cm)	m	λ_o (cm)	λ_g (cm)	
	8.02		3.855	25	3.741	4.000	3.625
2c=7.5	8.30		3.717	26	3.615	3.846	3.354
d=4.5	8.53		3.611	27	3.517	3.704	2.511
2a= 3	8.87		3.465	28	3.382	3.571	2.968
2h= 60	9.15		3.355	29	3.279	3.448	2.697
l= 50	9.42		3.254	30	3.185	3.333	2.370
	9.695		3.157	31	3.094	3.226	2.139
	9.975	15.52	3.066	32	3.008	3.125	1.888
	10.25		2.980	33	2.927	3.030	1.650
	10.54		2.895	34	2.846	2.941	1.564
	10.81		2.820	35	2.775	2.857	1.295
	11.085		2.748	36	2.706	2.778	1.079
	11.375		2.676	37	2.637	2.703	0.999
	11.67		2.607	38	2.571	2.632	0.949
	11.97		2.539	39	2.506	2.564	0.975
	12.26		2.501	40	2.469	2.500	0.040

X-band, it is seen that, as expected, the guides under test will have relatively low dispersion, because both wavelengths are within 1.3 percent and 6.5 percent, respectively, of each other.

When the measured moding spectra for different groove dimensions at 100 GHz were examined, there is little indication of higher order or rank modes:

a) for a plane separation of 10 and 12 mm and right-angled V-groove depths of 2 mm to 6 mm; and
b) when a 50 cm length of guide is distorted to give central plane separation up to 12 mm from 10 mm, or down to 6 mm.

An example of the moding spectrum at 100 GHz is shown in Fig. 13. The guide dimensions were optimized at

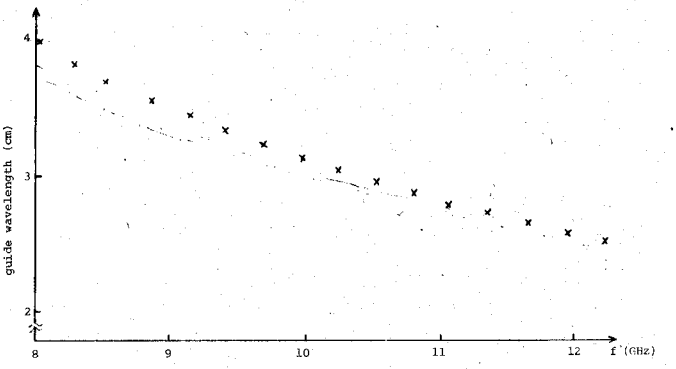

Fig. 12. Graph of guide wavelength versus frequency at *X*-band. —— Theoretical guide wavelength; × × × × × experimental guide wavelength; ·-·-·-· free-space wavelength.

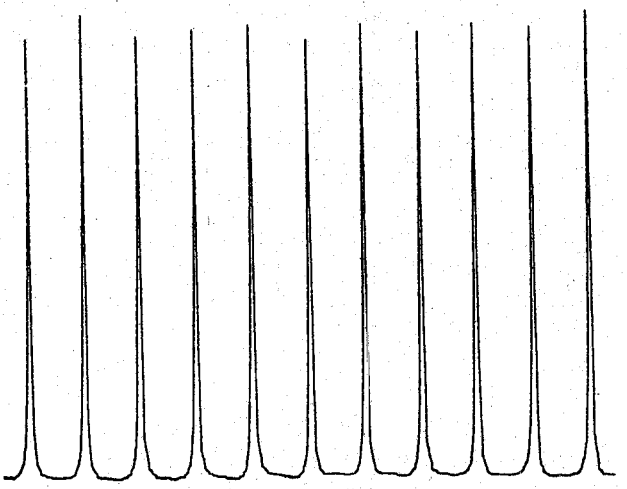

Fig. 13. Moding spectrum for a V-groove waveguide cavity of variable length at 100 GHz: $2c = 10$ mm, $2a = 6$ mm, $d = 3$ mm.

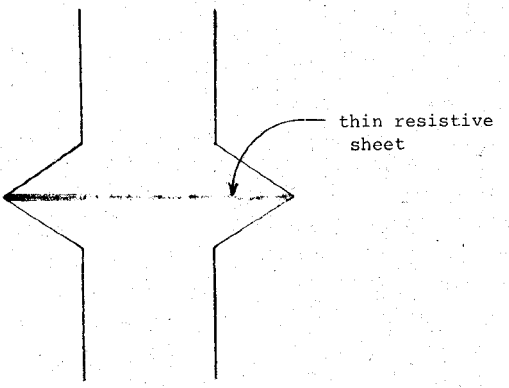

Fig. 14. Orthogonal mode filter of single V-groove guide.

X-band [6]:

$$2c \simeq 3\lambda_o, \quad d \simeq 0.6(2c), \quad 2a \simeq 0.4(2c), \quad 2h \geq 5(2c).$$

There seems no reason why these dimensions should not be used at 100 GHz.

Orthogonal modes (TE_e^f mode group [1]) can exist with relatively high Q factor (about a factor of two down on the required mode at 100 GHz) and the inclusion of the orthogonal mode filter is necessary. The guide wavelengths are 2 to 5 percent greater than the free-space wavelength at

TABLE III
LOSS CHARACTERISTIC OF SINGLE V-GROOVE GUIDE AT 100 MHz

2c (mm)	d (mm)	Q_ℓ ($\times 10^3$)	Q_u ($\times 10^4$)	α_g (dB/m)
10	2	6.7	2.3	0.4
	4	5.9	2.3	0.4
	6	6.4	1.5	0.6
12	2	8.5	1.8	0.5
	4	6.7	3.0	0.3
	6	8.1	2.3	0.4

100 GHz. A mode filter at 100 GHz has been constructed with good performance by including a thin metal sheet at the central level of the groove region (Fig. 14).

Experimental guide attenuation constants at 100 GHz are given in Table III. The experimental loss is shown to be from 0.3 to 0.6 dB/m (c.f. the dominant TE_{10} mode rectangular waveguide at 100 GHz (WG 28) constructed from silver has an experimental attenuation constant of 5 dB/m [7]). The mode filter has not been included in these measurements. No attempt has been made to minimize this loss by guide surface treatment.

Our conclusion from a wide range of experimental measurements at 100 GHz and at X-band is that the guide characteristics are very close to those predicted for dispersion. Dimensions are optimized for moding behavior. The attenuation measurements are also encouraging in that the experimental loss is relatively low, even for a guide constructed from aluminum by conventional workshop techniques.

V. CONCLUSIONS

A conformal mapping technique for single-groove guide has been discussed. The wave equation for grooves of arbitrary cross section has been given. With appropriate matching of boundary values, the scaling factor, $h(x, y)$, has been formulated for grooves of V-shaped cross section. Also, with appropriate boundary conditions to the assumed solution of the wave equation, the characteristic equation has been obtained. The open-type transformation, parameterization, and trapezoidal rule have been applied to evaluate numerically complex integrands with singularities which must be solved before $h(x, y)$ and the propagation characteristics can be found.

Experimental measurements at X-band and 100 GHz confirm that with appropriate choice of guide dimensions, the guide is low loss, low dispersion, single mode, and easy to manufacture. Theoretical analysis on the guide wavelength showed that the agreement to experimental results is very good.

The single V-groove guide has an advantage over its rectangular-groove counterpart for normal propagation since the attenuation is lower, the rejection of higher modes is more effective, and the orthogonal mode filter is easily constructed.

APPENDIX
FORMULATION OF THE SCALING FACTOR, $h(x, y)$

The scaling factor, $h(x, y)$, which is necessary for the determination of the propagation characteristics of single V-groove guide, has been given in Section II-B-1. This section describes the manipulation for obtaining the scale factor, $h(x, y)$, by a transformation from the V-shaped groove waveguide to a parallel-plate waveguide which is partially filled with a nonisotropic and nonuniform medium. The transformation would inevitably employ the upper half-plane as the intermediate step [8], [9].

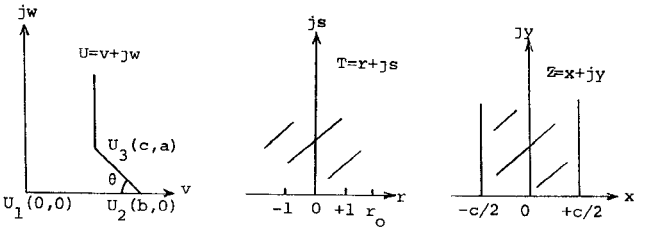

Fig. 15. Transformation planes from the V-groove guide to the H guide.

A. Schwartz–Christoffel Transformation and Boundary Value Matching

Consider one quarter of the cross section of the V-groove guide. The transformation from the V-groove guide to the parallel-wall guide involves the upper half-plane as the intermediate step. They are shown in Fig. 15. By the Schwartz–Christoffel theorem,

$$\frac{dU}{dT} = k_1(T-r_0)^{1/2-\theta/\pi}(T-1)^{\theta/\pi-1}(T+1)^{-1/2} \quad \text{(A1)}$$

and

$$\frac{dZ}{dT} = k_2(T-1)^{-1/2}(T+1)^{-1/2}. \quad \text{(A2)}$$

Consider the transformation from the T plane to the Z plane:

$$\frac{dZ}{dT} = \frac{k_2}{\sqrt{T^2-1}} = \frac{k}{\sqrt{1-T^2}}.$$

Hence $Z = k\sin^{-1}T + B$.

Matching boundary values at $T = \pm 1$ with $Z = \pm c/2$ (Fig. 15) gives

$$T = \sin(\pi Z/c).$$

Rearranging (A1) and (A2) yields

$$\frac{dU}{dZ} = k_3\left[\frac{T-r_0}{T-1}\right]^{1/2-\theta/\pi} \quad \text{(A3)}$$

where $k_3 = k_1/k_2$ and $k_2 = jk = jc/\pi$. Since $\theta/\pi < 1/2$, i.e., $\theta < \pi/2$, assume that U is a function of r only, i.e.,

$$U = f(r) = k_1\int_{-1}^{r}\frac{(T-r_0)^{1/2-\theta/\pi}}{(T-1)^{1-\theta/\pi}(T+1)^{1/2}}\,dT + k_4 \qquad (-1 \leqslant r \leqslant r_0)$$

$$= k_1\int_{-1}^{r} G(T)\,dT + k_4$$

where

$$G(T) = \frac{(T-r_0)^{1/2-\theta/\pi}}{(T-1)^{1-\theta/\pi}(T+1)^{1/2}}.$$

Matching boundary values at

$$r=-1 \quad \text{gives} \quad U=U_1(0,0)=U_1=k_4$$
$$r=+1 \quad \text{gives} \quad U=U_2(b,0)=U_2$$
$$r=r_0 \quad \text{gives} \quad U=U_3(c,a)=U_3$$
$$\therefore U_2-U_1=k_1\int_{-1}^{+1}G(T)\,dT \tag{A4}$$
$$U_3-U_1=k_1\int_{-1}^{r_0}G(T)\,dT. \tag{A5}$$

Hence

$$\frac{U_3-U_1}{U_2-U_1}=\frac{\int_{-1}^{r_0}G(T)\,dT}{\int_{-1}^{+1}G(T)\,dT}. \tag{A6}$$

Since the coordinates of U_1, U_2, and U_3 are known, r_0 can be determined from (A6). Also, since

$$h(x,y)=|dU/dZ|$$

and r_0 has been determined, $h(x,y)$ can be found from (A3). However, the integrands of the integrals in (A6) are complex and contain singularities at both lower and upper limits, and these singularities must be removed before integration can be performed numerically. These difficulties will be dealt with in the following sections.

B. Open-Type Transformation

In this subsection, the method of open-type transformation is used to remove the singularities. The integrands are partitioned into forms that can be transformed to a nonsingular integrand. Consider the following integral:

$$I=\int_{w_1}^{w_2}\frac{f(w)}{(w-w_1)^p}\,dw$$

where $w_2>w_1$. Clearly I has an integrand which has singularity at $w=w_1$. Let

$$z^\phi=w-w_1$$

where

$$\phi=\frac{1}{1-p}$$

i.e.,

$$\phi p=\phi-1$$

and

$$dw=\phi z^{\phi-1}\,dz.$$

When $w=w_1$, $z=0$ and when $w=w_2$, $z=z_1=(w_2-w_1)^{1/\phi}$. Therefore,

$$I=\int_0^{z_1}\frac{F(z)}{z^{\phi p}}\phi z^{\phi-1}\,dz$$
$$=\phi\int_0^{z_1}F(z)\,dz$$

where

$$F(z)=f(z^\phi+w_1).$$

After the above transformation, the integrand $f(w)/(w-w_1)^p$ with singularity at $w=w_1$ is transformed into an integrand, $F(z)$, which contains no singularity.

C. Parameterization

Although the integrand has no singularity after the open-type transformation, it is complex and multivalued. Integration of the complex variable requires splitting the complex integrand into real and imaginary parts. Let

$$G(T)=A(R,S)+jI(R,S)$$

i.e.,

$$\int_l G(T)\,dT=\int_l(A+jI)\,d(R+jS)$$
$$=\int_l(A\,dR-I\,dS)+j\int_l(I\,dR+A\,dS).$$

In parametric form, R and S can be written as

$$R=R(t)$$

and

$$S=S(t).$$

Then,

$$A=A(t)$$

and

$$I=I(t).$$

Therefore,

$$\int_l G(T)\,dT=\int_{t_1}^{t_2}\left[A(t)\dot{R}(t)-I(t)\dot{S}(t)\right]dt$$
$$+j\int_{t_1}^{t_2}\left[I(t)\dot{R}(t)+A(t)\dot{S}(t)\right]dt.$$

In this way, the parameterization has altered the integration to two real integrations of real variables. A carefully chosen path for integration is necessary because different paths of integration will usually give different results, owing to the fact that the paths may lie on different Riemann surfaces.

D. Evaluation of the Complex Integration

After introducing the open-type transformation and the parameterization shown in subsections *B* and *C*, let us consider the evaluation of the integrals on the right-hand side of (A6), namely

$$I_1=\int_{-1}^{r_0}G(T)\,dT$$
$$=\int_{-1}^{0}G(T)\,dT+\int_0^{+1}G(T)\,dT+\int_{+1}^{r_0}G(T)\,dT$$
$$=I_{21}+I_{22}+I_{11}$$
$$I_2=\int_{-1}^{+1}G(T)\,dT$$
$$=\int_{-1}^{0}G(T)\,dT+\int_0^{+1}G(T)\,dT$$
$$=I_{21}+I_{22}$$

where

$$G(T)=\frac{(T-r_0)^{1/2-\theta/\pi}}{(T-1)^{1-\theta/\pi}(T+1)^{1/2}}.$$

1) Evaluation of I_{11}: The integrand has singularity at $T=+1$. Following the transformation shown in subsection B and letting

$$f(T)=\frac{(T-r_0)^{1/2-\theta/\pi}}{(T+1)^{1/2}}$$

a nonsingular integrand is obtained. The integral is then separated into two real integrals using the method outlined in subsection C. The path of integration is chosen along the real axis ($R=t, S=0$) to obtain a simple parameterization. The integrand is multivalued and principal values of the integrand are used in the evaluation of the integral. The trapezoidal rule is used for the evaluation of the integration.

2) Evaluation of I_{21}: The integrand has singularity at $T=-1$. The method of integration is the same as that in subsection D-1 but with

$$f(T)=\frac{(T-r_0)^{1/2-\theta/\pi}}{(T-1)^{1-\theta/\pi}}.$$

3) Evaluation of I_{22}: The integrand, I_{22} in this case, has singularity at the upper limit, i.e. $T=+1$, which is not of the same type as that described in subsections D-1 and D-2, where the singularity occurs at the lower limit. If the same method is used to transform I_{22}, i.e., $z^{\phi}=T-1$, where $\phi=\pi/\theta$, the real axis in the T plane will be transformed into a straight line of finite slope in the upper half Z plane. This may give a wrong computation since points in the upper half Z plane usually lie in a Riemann surface different from those points in the real axis of the upper half Z plane. The transformation may be modified as follows. Let

$$f(T)=\frac{(T-r_0)^{1/2-\theta/\pi}}{(T+1)^{1/2}}$$

and

$$z^{\phi}=1-T$$

where

$$\phi=\frac{1}{1-p}$$

and

$$p=1-\theta/\pi.$$

Similar to the transformation shown in subsection B, an integral with a nonsingular integrand is obtained, i.e.,

$$z^{\phi}=1-T$$

where

$$\phi=\pi/\theta$$

$$T=1-z^{\phi}$$

i.e.,

$$dT=-\phi z^{\phi-1}\,dz.$$

When $T=0$, $z^{\phi}=1$, i.e. $z=1$ for $\phi\neq 0$, and when $T=1$, $z^{\phi}=0$, i.e. $z=0$ for $\phi\neq 0$:

$$I_{22}=\int_1^0\frac{(1-z^{\phi}-r_0)^{1/2-\theta/\pi}}{(2-z^{\phi})^{1/2}(-z^{\phi})^{1-\theta/\pi}}(-\phi)z^{\phi-1}\,dz$$

$$=\frac{\phi}{(-1)^{1-\theta/\pi}}\int_0^1\frac{(1-r_0-z^{\phi})^{1/2-\theta/\pi}}{(2-z^{\phi})^{1/2}}\,dz.$$

The significance lies in the fact that the real axis in the T plane is mapped to the real axis in the Z plane by this transformation. Again, the trapezoidal rule is used for the evaluation of the integration.

Having evaluated I_1 and I_2, r_0 can be determined by using (A6). Moreover, k_1 can be calculated from (A4) or (A5), in which

$$k_1=\frac{U_2-U_1}{\int_{-1}^{+1}G(T)\,dT}=\frac{U_3-U_1}{\int_{-1}^{r_0}G(T)\,dT}.$$

Hence

$$h(x,y)=\left|\frac{dU}{dZ}\right|=|k_3|\left|\left[\frac{T-r_0}{T-1}\right]^{1/2-\theta/\pi}\right|$$

where

$$k_3=\frac{k_1}{k_2}=\frac{k_1}{jc/\pi}$$

$$T=\sin\left(\frac{\pi}{c}Z\right)=\sin\left[\frac{\pi}{c}(x+jy)\right].$$

Therefore,

$$h(x,y)=|k_3|\left|\left[\frac{\sin\left[\frac{\pi}{c}(x+jy)\right]-r_0}{\sin\left[\frac{\pi}{c}(x+jy)\right]-1}\right]^{1/2-\theta/\pi}\right|.$$

References

[1] Y. M. Choi, "Groove guide as a short-millimetric waveguide system," Ph.D. thesis, University of Wales/UWIST., Apr. 1982.

[2] Y. M. Choi and K. F. Tsang, "Report 3," unpublished report to the Research Committee, Hong Kong Polytechnic, Oct. 1985.

[3] Y. M. Choi and D. J. Harris, "Groove guide for short millimetric waveguide systems," *Infrared and Millimeter Waves*, vol. 11, pp. 99–140, Dec. 1984.

[4] T. K. Ho and D. J. Harris, "Millimetric wave groove guide with V-shaped grooves," *Electron. Lett.*, vol. 20, no. 19, pp. 777–778, Sept. 1984.

[5] H. Y. Yee and N. F. Audeh, "Wave propagation in groove guides," in *Proc. 21st Nat. Electron. Conf.* (Chicago), Oct. 1965, pp. 18–23.

[6] Y. M. Choi and K. F. Tsang, "Optimization of dimensions of single V-groove guide," *Electron. Lett.*, vol. 21, no. 11, pp. 477–479, May 1985.

[7] F. J. Tischer, "Experimental attenuation of rectangular waveguide at millimeter wavelengths," *IEEE Trans. Microwave Theory Tech.*, vol. MTT-27, pp. 31–37, Jan. 1979.

[8] F. J. Tischer, "Conformal mapping in waveguide considerations," *Proc. IEEE*, vol. 51, pp. 1050–1051, July 1963.

[9] F. J. Tischer, "The groove guide, a low-loss waveguide for millimeter waves," *IEEE Trans. Microwave Theory Tech.*, vol. 11, pp. 291–296, Sept. 1963.

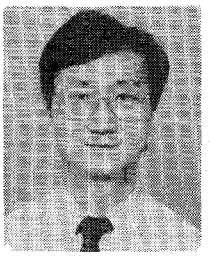

Yat Man Choi (M'83) graduated with the B.Eng. degree in electrical and electronic engineering with first class honours in 1978 and obtained the Ph.D. degree in 1982, both from the University of Wales Institute of Science and Technology (UWIST), United Kingdom.

He joined the Department of Electronic Engineering, Hong Kong Polytechnic, Hong Kong, in 1982 as a Lecturer. His teaching activities include communication engineering, microwave engineering, electromagnetic field theory, circuits and fields, and analog integrated circuits. In addition, he supervises laboratory groups and student projects. His present research centers on microwaves and millimeter waves.

Since 1986, he has been one of the degree course industry-based training tutors. Also, he was elected a member of the Academic Board of the Hong Kong Polytechnic in April 1987 and has been a departmental representative on the Polytechnic Staff Association since 1984. He was promoted from Lecturer to Senior Lecturer in September 1987.

Douglas J. Harris graduated in electrical engineering and obtained the Ph.D. degree from Queen Mary College, University of London.

Subsequent research and lecturing appointments were held at the Admiralty Laboratory, Baldock; Stanford University, Stanford, CA; Sheffield University; and Portsmouth Polytechnic. He was professor and head of the Department of Electrical Engineering at Ahmadu Bello University, Nigeria, for seven years and a visiting professor at University College London. He was also professor and head of the Department of Physics, Electronics and Electrical Engineering at the University of Wales Institute of Science and Technology, Cardiff, for ten years. Since 1985 he has been professor and head of the Department of Electrical and Communication Engineering, University of Technology, Lae, Papua New Guinea. His research interests have included high-voltage and microwave discharges, microwave electron tubes, m.h.d. generation, and atmospheric electricity, but his present research centers on millimeter and submillimeter waves.

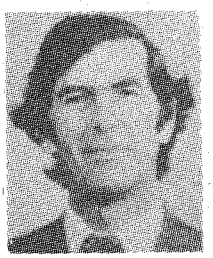

Kim-Fung Tsang received his Associateship in Electronic Engineering from the Hong Kong Polytechnic, Hong Kong, in 1983. He then joined the same department as a Research Assistant and simultaneously registered externally for the M.Eng. degree (by research) at the University of Wales Institute of Science and Technology, United Kingdom. His research area was V-groove waveguide and components.

In October 1985, he joined the department of Electronic Engineering, City Polytechnic of Hong Kong, Hong Kong. His research then dealt with groove guide and electromagnetic wave scattering problems. In September 1986 he joined Corad Technology Ltd. as a Product Executive responsible for microwave testing equipment and systems. He joined Hewlett Packard Hong Kong Ltd. in October 1987.